Front. Phys., 2014, 9(2): 226–233
DOI 10.1007/s11467-013-0406-9

RESEARCH ARTICLE

Current neutralization and plasma polarization for intense ion beams propagating through magnetized background plasmas in a two-dimensional slab approximation

Zhang-Hu Hu, Mao-Du Chen, You-Nian Wang†

School of Physics and Optoelectronic Technology, Dalian University of Technology, Dalian 116024, China

Corresponding author. E-mail: †ynwang@dlut.edu.cn

Received July 15, 2013; accepted November 18, 2013

A two-dimensional electromagnetic Particle-in-Cell (PIC) simulation model is proposed to study the propagation of intense ion beams with beam width w_b small compared to the electron skin depth c/ω_{pe} through background plasmas in the presence of external applied magnetic fields. The effective electron gyroradius w_{ge} is found to be an important parameter for ion beam transport in the presence of magnetic fields. In the beam regions, the background plasmas respond differently to the ion beam of width $w_b < w_{ge}$ and $w_b > w_{ge}$ for the given magnetic field and beam energy. For the case of beam width $w_b < w_{ge}$ with relative weak external magnetic fields, the rotation effects of plasma electrons are found to be significant and contributes to the significant enhancement of the self-electric and self-magnetic fields. While for the case of beam width $w_b > w_{ge}$ with relative strong external magnetic fields, the rotation effects of plasma electrons are strongly inhibited and a well neutralization of ion beam current can be found. Finally, the influences of different beam widths, beam energies and magnetic fields on the neutralization of ion beam current are summarized for the cases of $w_b < w_{ge} < c/\omega_{pe}$, $w_{ge} < w_b < c/\omega_{pe}$ and $w_b < c/\omega_{pe} < w_{ge}$.

Keywords current neutralization, ion beams, magnetized plasmas, Particle-in-Cell simulations

PACS numbers 52.40.Mj, 52.59.-f, 52.25.Xz

1 Introduction

The investigations of transport and focusing of charged ion beams have a variety of important applications, such as warm dense matter physics [1], high-energy-density physics [2–4], and the heavy ion fusion [5, 6]. For these applications, the ion beam should be simultaneously compressed in the transverse and longitudinal directions to small spot sizes and short pulses, respectively, due to the reason that the power per unit area that delivered by the beam to the target is inversely proportional to the square of beam radius and the pulse duration. Simulations [7–9] and experiments [10–12] have proven that background plasma can be provided as an ideal media for ion beam focusing and transport. The plasma electrons tend to neutralize the strong repulsive space-charge force of beam ions and provide a good compression. In addition, the plasma lens has been proposed as a final focusing element to improve the luminosity of future high energy electron-positron colliders [13].

The propagation of an intense ion beam pulse through the background plasma has been investigated theoretically through the warm-fluid [14], kinetic [15], hybrid fluid-Vlasov [16], and Particle-in-Cell (PIC) simulations [7–9]. It is shown that for long, nonrelativistic ion beams, charge neutralization is complete even for very tenuous background plasmas. The background plasma can provide the necessary very high degree of neutralization for drift compression of intense ion beam pulses, provided the plasma density exceeds the beam density everywhere along the beam path. Experiments have shown that a 60-fold longitudinal pulse compression of ion beams can be achieved by applying a time-dependent velocity tilt to the charge bunch and subsequently allowing it to drift through a background plasma [5]. The gas ionization by the beam ions improves the neutralization and leads to considerable enhancement of the self-magnetic field in the tail of the beam pulse.

In addition, the application of a solenoidal magnetic

field along the beam propagation direction is found to show significant effects on the properties of beam focusing [17, 18]. The magnitude of the self-electric field increases significantly as the value of external magnetic field increases from $\omega_{ce} < 2\beta_b\omega_{pe}$ to $\omega_{ce} \gg 2\beta_b\omega_{pe}$, providing an enhanced focusing of the beam pulse. Here, $\omega_{ce} = eB_0/(m_e c)$ is the electron cyclotron frequency, $\omega_{pe} = (4\pi n_0 e^2/m_e)^{1/2}$ is the electron plasma frequency, and $\beta_b = v_b/c$ with v_b the beam velocity and c the speed of light. For relativistic beams, the application of a solenoidal magnetic field strongly affects the degree of current and charge neutralizations when $\omega_{ce} > \gamma_b\beta_b\omega_{pe}$, where $\gamma_b = (1-\beta_b^2)^{-1/2}$. The threshold value of the applied magnetic field $\gamma_b\beta_b\omega_{pe}$ is relatively small for nonrelativistic beams, while for relativistic ion beams this threshold value could be large. There are many important parameters for ion beam transport in background plasmas, including beam energy, beam and plasma density profile, type of ion species and gas ionization, etc. Thus, an extensive study is needed for a wide range of beam and plasma parameters to determine the condition for optimum beam propagation.

We adopt in this work a two-dimensional relativistic, electromagnetic PIC simulation method to investigate the propagation of intense ion beams with beam width small compared to the electron skin depth $w_b < c/\omega_{pe}$ through background plasmas in the presence of magnetic fields, taking into account the relativistic effects. Influences of beam width and energy on the neutralization of beam current and plasma polarization are investigated in detail. The paper is organized as follows. In Section 2, the two-dimensional relativistic, electromagnetic PIC simulation method is briefly described. Simulation results are analyzed in detail in Section 3. Finally, we give a short summary in Section 4.

2 PIC simulation methods

Consider a two-dimensional plasma slab model shown in Fig. 1. The magnetic field B_0 applied in the plasma is homogeneous and directed along the x axis. The simulation region extends spatially from $X = 0$ to $X = L_x$ and from $Y = 0$ to L_y. Initially, the plasma of density n_0 is placed between $L_x/10$ and L_x with the other regions be vacuum. The beam ions are injected from the left boundary and propagate along the x direction. The equations of motions for charged particles are

$$\frac{d\boldsymbol{s}}{dt} = \boldsymbol{v} \tag{1}$$

$$\frac{d\boldsymbol{u}}{dt} = \frac{q}{m_0}\left(\boldsymbol{E} + \frac{\boldsymbol{u}\times\boldsymbol{B}}{\gamma c}\right) \tag{2}$$

where $\boldsymbol{s}, \boldsymbol{v}, q$ and m_0 are the position, velocity, charge and rest mass of charged particles, respectively. Here $\boldsymbol{u} = \gamma\boldsymbol{v}$ with $\gamma = \sqrt{1+u^2/c^2}$, c is the speed of light, and $\boldsymbol{E}$ and $\boldsymbol{B}$ are the electric and magnetic fields, which are determined by Maxwell's equations:

$$\partial_t\boldsymbol{B} = -c\nabla\times\boldsymbol{E}, \quad \partial_t\boldsymbol{E} = c\nabla\times\boldsymbol{B} - 4\pi\boldsymbol{J} \tag{3}$$

$$\nabla\cdot\boldsymbol{B} = 0, \quad \nabla\cdot\boldsymbol{E} = 4\pi\rho \tag{4}$$

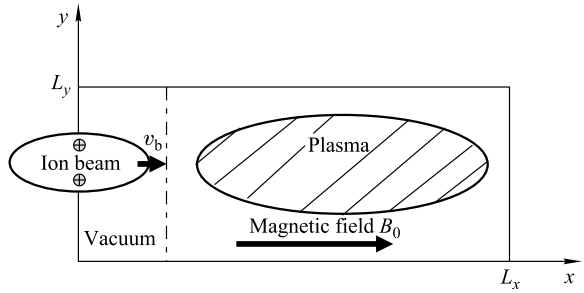

Fig. 1 A two-dimensional plasma slab model.

A 2D3V relativistic, electromagnetic PIC code is used for the simulation. The field equation (3) is solved with an alternating-direction implicit (ADI) finite-difference time-domain (FDTD) method [19] to eliminate the restraint of the CFL condition. The numerical integration of the equations of motions for all charged particles is performed by a standard leap-frog algorithm, with the Lorentz forces treated by the Boris rotation [20]. Periodic boundary condition in the y direction and perfectly matched layer (PML) [21] absorbing boundary condition in the x direction are adopted. To reduce the computation cost, a moving-window approach is used in the simulation, where the window of the simulation travels at the speed of light. The code is parallelized using message passing interface (MPI) through domain decomposition. Also, for the efficiency of parallel computation, a current deposition scheme [22] is designed to conserve charge exactly and there is no need to solve Poisson's equation.

In our numerical simulations, a hydrogen plasma with mass ratio $m_p/m_e = 1836$ and plasma ion charge $Z_p = e$ is considered. Also the injection beam ions are taken to be proton with mass $m_b = 1836m_e$ and charge $Z_b = e$. Plasma parameters used in the simulation are as follows: unperturbed plasma density $n_0 = 10^{11}$ cm^{-3} and initial plasma electron temperature $T_{e0} = 4$ eV. Then the skin depth c/ω_{pe} is shown to be 1.68 cm. The magnetic field B_0 and beam injection velocity v_b are treated as variables. The simulation box is composed of $N_x = 8000$ grids in the x direction and $N_y = 1024$ grids in the y direction. The space step dx and time step dt are fixed to 6×10^{-3} cm and $(0.2\text{–}0.3)\times10^{-12}$ s for stability. Thus, the lengths of the simulation region L_x and L_y are 48 cm

and 6.1 cm, respectively. We have adopted averaged 20 superparticles per cell for each species, which has been varied to check the stability of the results.

3 Current neutralization and plasma polarization

3.1 Beam width $w_b < w_{ge}$

Beam width is an important parameter for ion beam transport in background plasmas. Without external applied magnetic fields, the beam current is almost unneutralized and the self-magnetic field is a maximum when the beam width w_b is small compared to the electron skin depth c/ω_{pe}. Further, the positive charge of the ion beam is shown to be overcompensated by the plasma electron if a moderately weak solenoidal magnetic field satisfying $\omega_{ce} \gg \beta_b\omega_{pe}$ is applied along the beam propagation direction, as indicated in Ref. [18]. Here, the beam width should satisfy $w_b \gg w_{ge} = \frac{V_b}{\omega_{ce}}(1+\omega_{ce}^2/\omega_{pe}^2)^{1/2}$, i.e., the beam width should be large compared to the effective electron gyroradius w_{ge}. We will show in the following that the effective electron gyroradius w_{ge} is an important parameter for ion beam transport in background plasmas in the presence of external applied longitudinal magnetic fields. Taking into account the relativistic effects, the effective electron gyroradius becomes

$$w_{ge} = v_b(\gamma_b^2/\omega_{ce}^2 + 1/\omega_{pe}^2)^{1/2} = \frac{c}{\omega_{pe}}\sqrt{\frac{\beta_b^2\gamma_b^2}{\omega_{ce}^2/\omega_{pe}^2} + \beta_b^2} \quad (5)$$

where $\gamma_b = (1-\beta_b^2)^{-1/2}$ and $\beta_b = v_b/c$.

We first show the influences of different magnetic fields on the neutralization of ion beam current and the generated self-electric and magnetic fields for beam width $w_b < w_{ge}$. A Gaussian proton beam with density profile $n_b = 0.5n_p\exp[-(y-L_y/2)^2/w_b^2 - (x-v_bt)^2/l_b^2]$, beam width $w_b = 0.18c/\omega_{pe}$, and half length $l_b = 2c/\omega_{pe}$ propagating with velocity $v_b = 0.33c$ is assumed. The unperturbed plasma density n_p and temperature T_{e0} are taken to be 10^{11} cm^{-3} and 4 eV, respectively, as described in Section 2. Here, to acquire a good charge neutralization, the length l_b of ion beam is adopted to ensure that the beam pulse duration is much longer than the electron plasma period [9], i.e., $\tau_b\omega_{pe} \gg 2\pi$.

Figure 2 shows the on-axis distribution of longitudinal current density along the beam propagation direction for different magnetic fields at time $t = 2240/\omega_{pe}$. The density distribution of ion beam is also shown in the figure for comparison. In addition, relative weak magnetic fields ($\omega_{ce}/\omega_{pe} \leqslant 1$) are adopted in the simulation ($B_0 = 600$ G and 1500 G) for the case of $w_b < w_{ge}$. It is clearly seen that for beam width $w_b < w_{ge}$ the magnetic field is deleterious for the neutralization of ion beam current. As the magnetic field increases, the longitudinal current in the beam regions ($en_bv_b - en_ev_{ex}$) increases and the magnitudes of generated self-magnetic and electric fields increase significantly, as shown in Figs. 3 and 4, where the azimuthal component of the self-magnetic field B_φ and transverse component of the self-electric field E_y are displayed. In addition, the circle with dashed line in the figure shows the outline of the ion beam. The self-magnetic and electric fields are seen to increase from

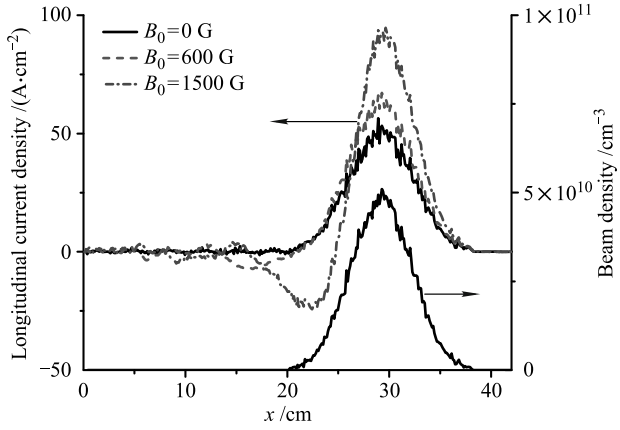

Fig. 2 The on-axis distribution of longitudinal current density (in unit of A/cm^2) along the beam propagation direction for different magnetic fields at time $t = 2240/\omega_{pe}$. The density distribution of ion beam (in unit of cm^{-3}) is also shown in the figure for comparison. A Gaussian proton beam with density profile $n_b = 0.5n_p\exp[-(y-L_y/2)^2/w_b^2 - (x-v_bt)^2/l_b^2]$, beam width $w_b = 0.18c/\omega_{pe}$, and half length $l_b = 2c/\omega_{pe}$ propagating with velocity $v_b = 0.33c$ is assumed. The unperturbed plasma density n_p and temperature T_{e0} are taken to be 10^{11} cm^{-3} and 4 eV, respectively.

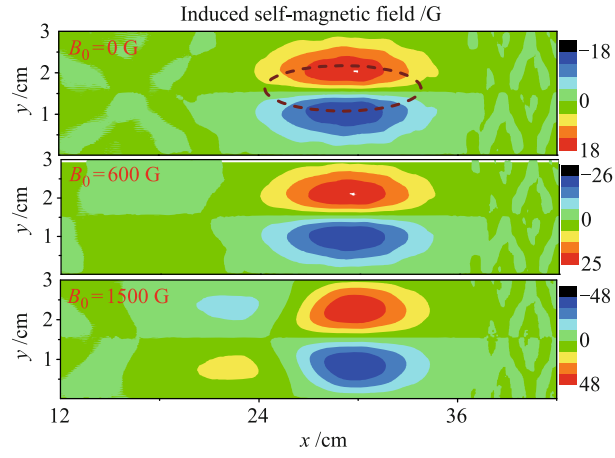

Fig. 3 The corresponding azimuthal component of the self-magnetic field B_φ (in unit of G) for different external applied magnetic fields with the same parameters as in Fig. 2. The circle with dashed line in the figure shows the outline of ion beam.

18 G and 1.2 kV/cm at the external magnetic field B_0 = 0 G to 47 G and 33 kV/cm at B_0 = 1500 G. This significant increase in the self-electric and magnetic fields is due to the rotations of plasma electrons about the beam axis with a high azimuthal velocity [17]. This rotation effect is caused by the inward transverse motion of plasma electrons. Also, the enhancement of longitudinal current with increasing external applied magnetic fields can also be explained by the rotation effects of plasma electrons.

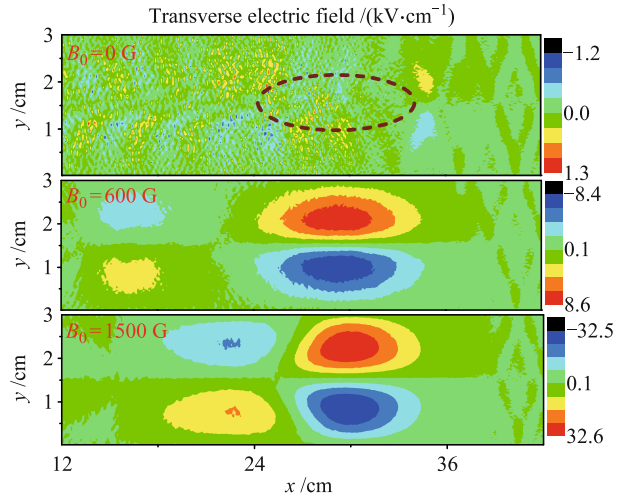

Fig. 4 The corresponding transverse component of the self-electric field E_y (in unit of kV/cm) for different external applied magnetic fields with the same parameters as in Fig. 2. Also, the circle with dashed line in the figure shows the outline of ion beam.

This rotation effects can be observed from the transverse azimuthal current density distribution of plasma electrons, as shown in Fig. 5 for external magnetic fields B_0 = 600 G and 1500 G at time $t = 2240/\omega_{pe}$ with other parameters the same as in Fig. 2. This transverse current further induces a positive longitudinal magnetic field, leading to the enhancement of longitudinal magnetic field inside the ion beam, as indicated in Fig. 6, where the on-axis distribution of perturbed longitudinal magnetic field δB_x is displayed. From this figure, the combined ion beam-plasma system is seen to act as a paramagnetic medium for the case of beam width $w_b < w_{ge}$. In the absence of an applied magnetic field, the ion beam is focused by the self-magnetic field due to the unneutralized beam current. Although the self-magnetic and electric fields increase significantly as a longitudinal magnetic field applies, the transverse electric force increases more rapidly than the magnetic force and the transverse force acting on the beam ions $F_y = e(E_y - v_b B_\varphi)$ can change sign from focusing to defocusing, as indicated in Fig. 4.

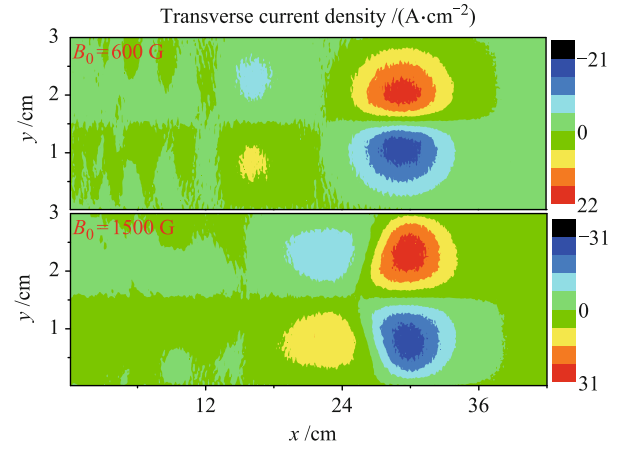

Fig. 5 The transverse azimuthal current density distribution (in unit of A/cm^2) for external magnetic fields B_0 = 600 G and 1500 G at time $t = 2240/\omega_{pe}$ with other parameters the same as in Fig. 2.

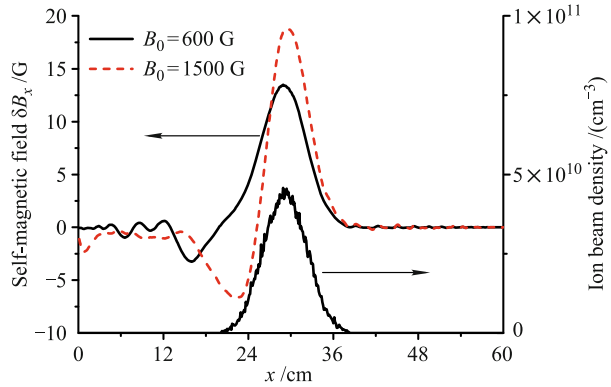

Fig. 6 The on-axis distribution of perturbed longitudinal magnetic field (in unit of G) along the beam propagation direction for external magnetic fields B_0 = 600 G and 1500 G at time $t = 2240/\omega_{pe}$ with other parameters the same as in Fig. 2. The on-axis distribution of ion beam density is also displayed in the figure for comparison.

3.2 Beam width $w_b > w_{ge}$

We further show the influences of different magnetic fields on the current neutralization and plasma polarization for beam width $w_b = 0.43c/\omega_{pe} > w_{ge}$, with other beam and plasma parameters the same as those in Fig. 2. Figure 7 shows the on-axis distribution of longitudinal current density along the beam propagation direction for different magnetic fields at time $t = 2240/\omega_{pe}$. Also, the corresponding ion beam density is displayed in the figure for comparison. Relative strong magnetic fields ($\omega_{ce}/\omega_{pe} > 1$) are selected for the simulation (B_0 = 2000 G and 10^4 G) to ensure the condition $w_b > w_{ge}$, as indicated in Eq. (5). One can clearly see from the figure that the longitudinal current in the beam regions reduces significantly as the magnetic field increases, indicating the well neutralization of ion beam

current. Here, the beam pulse duration $2l_b/v_b$ is much longer that the electron plasma period $2\pi/\omega_{pe}$ and a good charge neutralization can be acquired. With this condition, one cam assume the quasineutrality condition holds, $n_e \cong n_p + Z_b n_b$, where n_e is the plasma electron density, n_p the density of background plasma ions and $Z_b e$ is the ion charge of beam ions, whereas $Z_b = 1$ for proton beams. With strong applied longitudinal magnetic fields, the transverse transports of plasma electrons are strongly inhibited and plasma electrons move freely along the magnetic field lines. In this case, the motion of plasma electrons can be considered to be one-dimensional (along the beam propagation direction). Then with the charge density continuity equation, $\partial\rho/\partial t + \nabla \cdot \boldsymbol{J} = \partial\rho/\partial t + \partial J_x/\partial z = 0$, and the quasineutrality condition ($\rho = e(n_p + Z_b n_b - n_e) \cong 0$), one can obtain $J_x \cong 0$. Thus, plasma electrons tend to neutralize the beam current. Then plasma electrons ahead and in the tail of the beam pulse are attracted toward the ion beam, leading to the generation of positive and negative longitudinal current ahead and in the tail of the beam pulse, as indicated in Fig. 7.

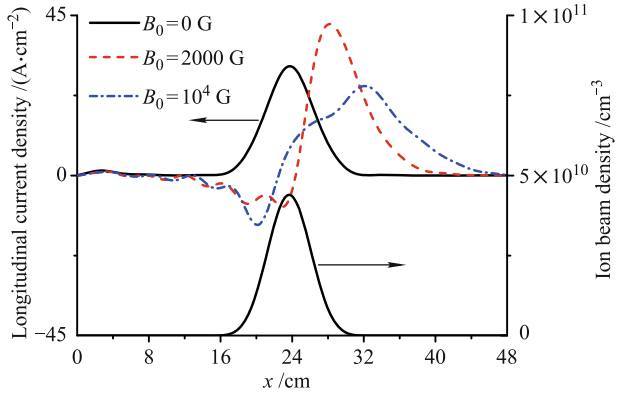

Fig. 7 The on-axis distribution of longitudinal current density (in unit of A/cm^2) along the beam propagation direction for different magnetic fields at time $t = 1680/\omega_{pe}$ for beam width $w_b = 0.43c/\omega_{pe}$ with other parameters the same as in Fig. 2.

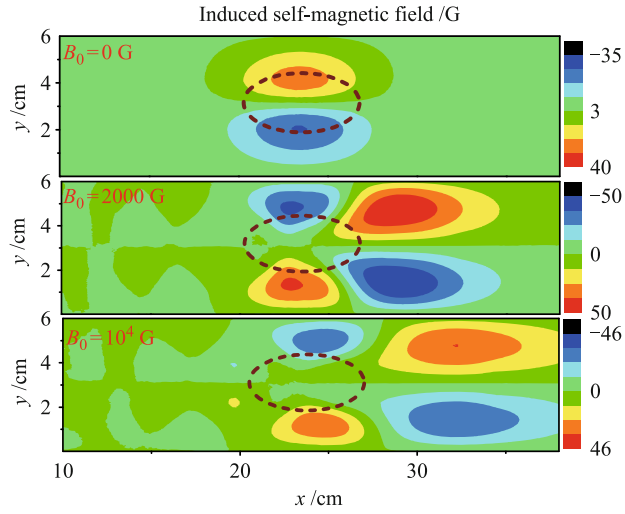

Fig. 8 The corresponding azimuthal component of the self-magnetic field B_φ (in unit of G) for different external applied magnetic fields with the same parameters as in Fig. 7. The circle with dashed line in the figure shows the outline of ion beam.

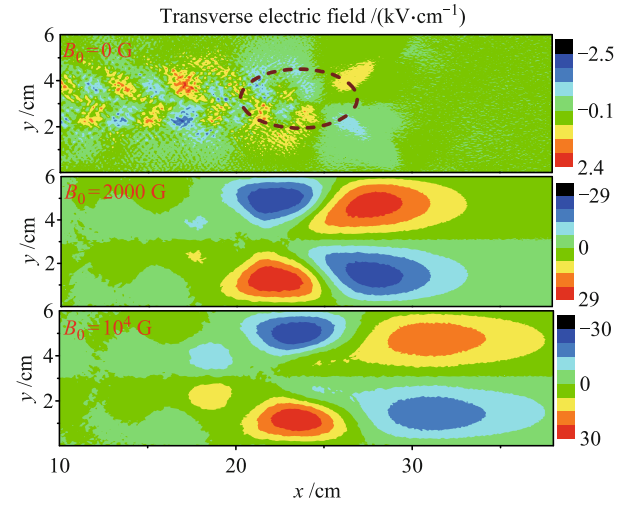

Fig. 9 The corresponding transverse component of the self-electric field E_y (in unit of kV/cm) for different external applied magnetic fields with the same parameters as in Fig. 7. Also, the circle with dashed line in the figure shows the outline of ion beam.

The corresponding azimuthal component of self-magnetic field B_φ and transverse component of self-electric field E_y are also shown in Figs. 8 and 9, respectively. It is interesting to note that the generated self-electric and magnetic fields change direction near the position of beam head, which is determined by the distribution of longitudinal current shown in Fig. 7. In addition, the generated self-magnetic and electric fields in the beam regions also change the polarity compared to the case of no external magnetic field and the case of small beam width $w_b < w_{ge}$ with relative weak external magnetic fields, as shown in Figs. 3 and 4. The transverse electric force now focus the beam ions, as indicated in Fig. 10, where the transverse dependence of beam density and transverse electric field E_y on the beam center are displayed. The transverse focusing electric fields in Fig. 9 for the cases of $B_0 = 2000$ G and 10^4 G are shown to be 10 times larger than that of case $B_0 = 0$ G. This significant increase in the magnitude of transverse electric field indicates the enhanced focusing of ion beams in background plasmas. Besides, the generation of focusing electric field indicates the overcompensation of positive ion beam charge by plasma electrons [18]. For the case of beam width $w_b > w_{ge}$, the strong external magnetic fields are seen to reduce the azimuthal rotation of plasma electrons, which can be observed from Fig. 11, where

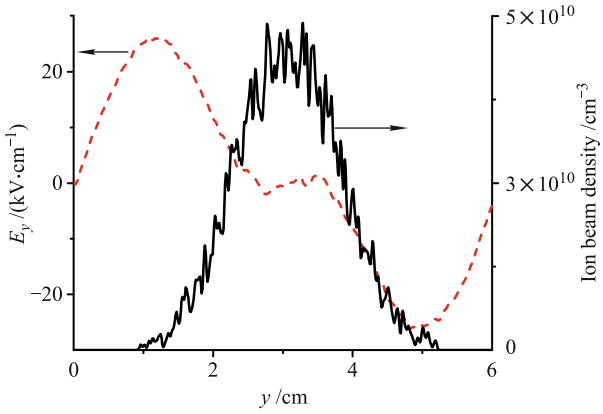

Fig. 10 The transverse dependence of beam density (in unit of cm^{-3}) and transverse electric field E_y (in unit of kV/cm) on the beam center in the case of magnetic field $B_0 = 2000$ G with beam and plasma parameters the same as in Fig. 7.

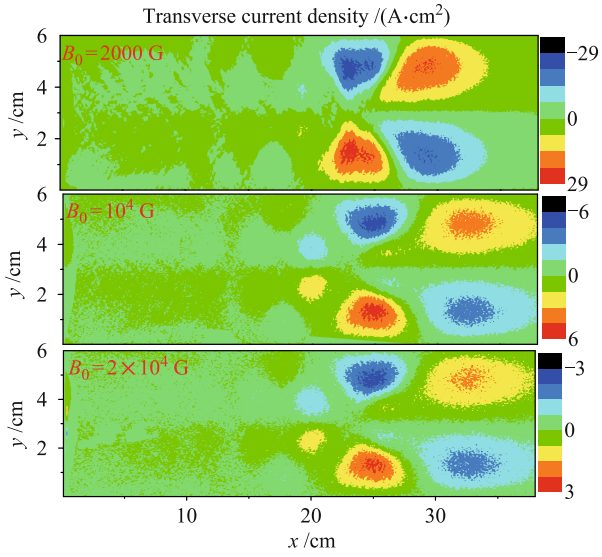

Fig. 11 The transverse azimuthal current density distribution (in unit of A/cm^2) for strong external magnetic fields at time $t = 1680/\omega_{pe}$ with beam and plasma parameters the same as in Fig. 7.

the transverse azimuthal current density distribution of plasma electrons is displayed for different magnetic fields with beam and plasma parameters the same as those in Fig. 7. In the figure, the significant reduce in the transverse current with increasing magnetic field is due to the strongly inhibited inward transverse motions of plasma electrons, which further leads to the significant reduce in the perturbed longitudinal magnetic field δB_x. Figure 12 further shows the on-axis distribution of longitudinal perturbed magnetic fields δB_x for different external applied magnetic fields B_0. The density distribution of ion beam is also displayed in the figure for comparison. We note in the figure the reduced magnitude of δB_x with increasing external magnetic fields, in contrast to the case shown in Fig. 6 for the case of beam width $w_b < w_{ge}$, where a revised behavior can be observed. In addition, the longitudinal magnetic field now is reduced inside the ion beam while enhanced in the front of ion beam.

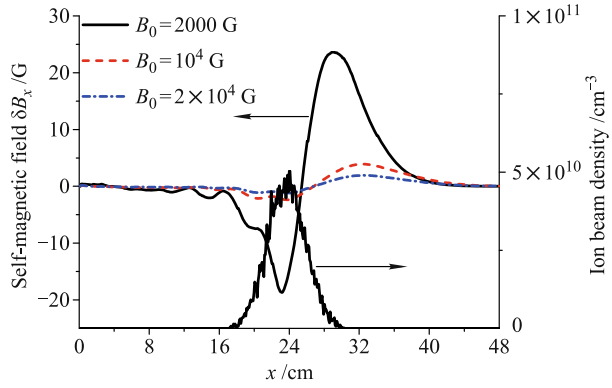

Fig. 12 The on-axis distribution of perturbed longitudinal magnetic field (in unit of G) along the beam propagation for strong external magnetic fields at time $t = 1680/\omega_{pe}$ with beam and plasma parameters the same as in Fig. 7. The on-axis distribution of ion beam density is also displayed in the figure for comparison.

For the magnetic fields we adopted in the simulations, the excitation of electromagnetic wave perturbations (e.g., Whistler waves) occurs, as discussed in detail by Dorf [23]. We have also tried in the simulations the conducting wall boundary condition in the transverse direction and made comparisons with the periodic boundary case. Complex wave-field structure can be observed for the conducting-wall boundary condition. However, there are no significant differences in the magnitude of longitudinal current near the ion beam regions and in the influences of different magnetic fields on the ion beam current neutralization for two boundary condition cases. Our further attention will focus on the electromagnetic wave excitation excited by the ion beam pulse in background plasmas, with the conducting-wall transverse boundary condition in the PIC code.

From Eq. (5), the effective electron gyroradius w_{ge} is seen to increase with the beam energy. For relativistic ion beams, w_{ge} can be larger than the electron skin depth c/ω_{pe} when the external applied magnetic field satisfies $\omega_{ce}/\omega_{pe} < \gamma_b\sqrt{\gamma_b^2-1}$. Eq. (5) can be further expressed as $w_{ge} = \frac{c}{\omega_{pe}}\sqrt{1+\frac{\gamma_b^2-1}{\omega_{ce}^2/\omega_{pe}^2}-\frac{1}{\gamma_b^2}}$. Then for w_{ge} to be smaller than c/ω_{pe}, the magnetic field and beam energy should satisfy $\frac{\gamma_b^2-1}{\omega_{ce}^2/\omega_{pe}^2} < \frac{1}{\gamma_b^2}$, i.e., $\omega_{ce}/\omega_{pe} > \gamma_b\sqrt{\gamma_b^2-1}$. Further simulations are performed for ion beams propagation through plasmas with different beam energies, beam widths and magnetic fields. The influences of these parameters on the ion beam current neutralization and plasma polarization are summarized in Fig. 13, where

the relationships between the w_{ge} and c/ω_{pe} are shown for different magnetic fields (ω_{ce}/ω_{pe}) and beam energies γ_b. The solid line in the figure indicates the case of $w_{ge} = c/\omega_{pe}$ obtained from $\omega_{ce}/\omega_{pe} = \gamma_b\sqrt{\gamma_b^2 - 1}$. For the given magnetic field and beam energy, the squares and circles below and up the solid line indicates the cases of $w_{ge} > c/\omega_{pe}$ and $w_{ge} < c/\omega_{pe}$, respectively. Also for each given magnetic field and beam energy, the neutralization of ion beam current is investigated in detail for different beam widths ($w_b < c/\omega_{pe}$). Simulation results show that for the case of $w_{ge} > c/\omega_{pe}$, the external applied magnetic fields in the ranges of $\omega_{ce}/\omega_{pe} < \gamma_b\sqrt{\gamma_b^2 - 1}$ are found to be deleterious for ion beam current neutralization, and enhance the self-electric and self-magnetic fields in background plasma significantly, due to the reason $w_b < c/\omega_{pe} < w_{ge}$, similar to the case shown in Fig. 2. While for the case of $w_{ge} < c/\omega_{pe}$, the beam width can be varied into regions of $w_b < w_{ge} < c/\omega_{pe}$ and $w_{ge} < w_b < c/\omega_{pe}$. Simulation results show that a well neutralization of ion beam current can be obtained for the magnetic fields $\omega_{ce}/\omega_{pe} \gg \gamma_b\sqrt{\gamma_b^2 - 1}$ provided the beam width $w_{ge} < w_b < c/\omega_{pe}$. For example, for an ion beam propagating through plasmas with velocity $v_b = 0.7c$ ($\gamma_b = 1.4$), the magnetic fields with the magnitude below the solid line ($\omega_{ce}/\omega_{pe} < \gamma_b\sqrt{\gamma_b^2 - 1}$) in the figure are found to reduce the neutralization of ion beam current for beam width $w_b < c/\omega_{pe}$. On the other hand, with the given beam energy, the magnetic fields up the solid line with the magnitude ($\omega_{ce}/\omega_{pe} \gg \gamma_b\sqrt{\gamma_b^2 - 1}$) are found to enhance the current neutralization for the beam width $0.65c/\omega_{pe}$ ($> w_{ge}$).

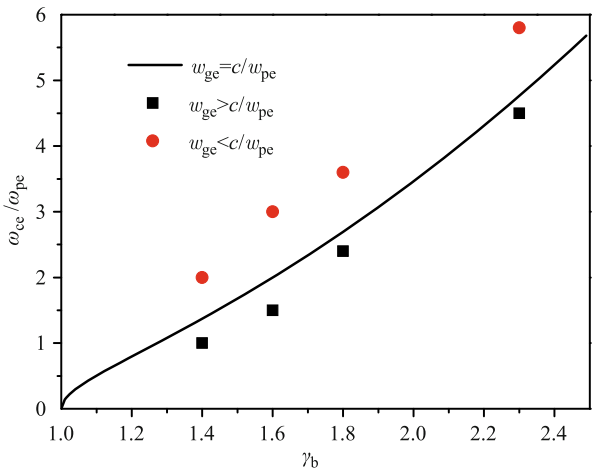

Fig. 13 Relationships between the w_{ge} and c/ω_{pe} for different magnetic fields (ω_{ce}/ω_{pe}) and beam energies γ_b. The solid line in the figure indicates the case of $w_{ge} = c/\omega_{pe}$ obtained from $\omega_{ce}/\omega_{pe} = \gamma_b\sqrt{\gamma_b^2 - 1}$. For the given magnetic field and beam energy, the squares and circles below and up the solid line indicates the cases of $w_{ge} > c/\omega_{pe}$ and $w_{ge} < c/\omega_{pe}$, respectively.

4 Summary

In summary, we have performed two-dimensional electromagnetic, relativistic PIC simulations to investigate the current neutralization and plasma polarization for intense ion beams with beam width small compared to the electron skin depth c/ω_{pe} propagating through background plasmas in the presence of external applied magnetic fields. The effective electron gyroradius $w_{ge} = v_b(\gamma_b^2/\omega_{ce}^2 + 1/\omega_{pe}^2)^{1/2}$ is found to play an important role in the ion beam current neutralization and plasma polarization. In the beam regions, the background plasmas respond differently to the intense ion beam of width $w_b < \omega_{ge}$ and $w_b > \omega_{ge}$ for the given magnetic field and beam energy.

For the case of beam width $w_b < \omega_{ge}$ with relative weak external magnetic fields, the rotation effects of plasma electrons are found to be significant, which are caused by the inward transverse motions of plasma electrons, and contribute to the significant enhancement of the self-electric and magnetic fields. Enhanced longitudinal current in the ion beam regions can be observed with increasing external magnetic fields. The combined ion beam-plasma system is seen to act as a paramagnetic medium, i.e., the longitudinal magnetic field is enhanced inside the ion beam.

While for the case of beam width $w_b > \omega_{ge}$ with relative strong external magnetic fields, the rotation effects of plasma electrons are found to be strongly inhibited and contribute to the significant reduce in the transverse current and longitudinal self-magnetic field. The current of the ion beam is found to be well neutralized. The longitudinal magnetic field now is reduced inside the ion beam, while enhanced in the front of ion beam. For relativistic ion beams, the well neutralization of ion beam current may not be obtained with small external applied magnetic fields $\omega_{ce} \leqslant \beta_b\gamma_b\omega_{pe}$ for the case of beam width small compared to the electron skin depth c/ω_{pe}. Finally, the influences of different beam widths, beam energies and magnetic fields on the neutralization of ion beam current are summarized for the cases of $w_b < w_{ge} < c/\omega_{pe}$, $w_{ge} < w_b < c/\omega_{pe}$ and $w_b < c/\omega_{pe} < w_{ge}$.

Acknowledgements This work was supported by the National Basic Research Program of China (Grant No. 2010CB832901), the National Natural Science Foundation of China (Grant No. 11305024), China Postdoctoral Science Foundation (Grant No. 2013M540219), and the Fundamental Research Funds for the Central Universities (Grant No. DUT13RC(3)25).

References

1. A. Ng, T. Ao, F. Perror, M. W. C. Dharma-Wardana, and

M. E. Foord, Idealized slab plasma approach for the study of warm dense matter, *Laser Part. Beams*, 2005, 23(04): 527

2. R. P. Drake, High-Energy-Density Physics, Berlin: Springer-Verlag, 2006
3. N. A. Tahir, D. H. H. Hoffmann, A. Kozyreva, A. Shutov, J. A. Maruhn, U. Neuner, A. Tauschwitz, P. Spiller, and R. Bock, Shock compression of condensed matter using intense beams of energetic heavy ions, *Phys. Rev. E*, 2000, 61(2): 1975
4. N. A. Tahir, D. H. H. Hoffmann, A. Kozyreva, A. Shutov, J. A. Maruhn, U. Neuner, A. Tauschwitz, P. Spiller, and R. Bock, Equation-of-state properties of high-energy-density matter using intense heavy ion beams with an annular focal spot, *Phys. Rev. E*, 2000, 62(1): 1224
5. P. K. Roy, S. S. Yu, E. Henestroza, A. Anders, F. M. Bieniosek, J. Coleman, S. Eylon, W. G. Greenway, M. Leitner, B. G. Logan, W. L. Waldron, D. R. Welch, C. Thoma, A. B. Sefkow, E. P. Gilson, P. C. Efthimion, and R. C. Davidson, Drift compression of an intense neutralized ion beam, *Phys. Rev. Lett.*, 2005, 95(23): 234801
6. S. S. Yu, R. P. Abbott, R. O. Bangerter, J. J. Barnard, R. J. Briggs, D. Callahan, C. M. Celata, R. Davidson, C. S. Debonnel, S. Eylon, A. Faltens, A. Friedman, D. P. Grote, P. Heitzenroeder, E. Henestroza, I. Kaganovich, J. W. Kwan, J. F. Latkowski, E. P. Lee, B. G. Logan, P. F. Peterson, D. Rose, P. K. Roy, G. L. Sabbi, P. A. Seidl, W. M. Sharp, and D. R. Welch, Heavy ion fusion (HIF) driver point designs, *Nucl. Instrum. Methods Phys. Res. A*, 2005, 544(1–2): 294
7. I. D. Kaganovich, G. Shvets, E. Startsev, and R. C. Davidson, Nonlinear charge and current neutralization of an ion beam pulse in a pre-formed plasma, *Phys. Plasmas*, 2001, 8(9): 4180
8. D. R. Welch, D. V. Rose, B. V. Oliver, and R. E. Clark, Simulation techniques for heavy ion fusion chamber transport, *Nucl. Instrum. Methods Phys. Res. A*, 2001, 464(1–3): 134
9. I. D. Kaganovich, E. Startsev, and R. C. Davidson, Nonlinear plasma waves excitation by intense ion beams in background plasma, *Phys. Plasmas*, 2004, 11(7): 3546
10. E. Henestroza, S. Eylon, P. Roy, S. Yu, A. Anders, F. Bieniosek, W. Greenway, B. Logan, R. MacGill, D. Shuman, D. Vanecek, W. Waldron, W. Sharp, T. Houck, R. Davidson, P. Efthimion, E. Gilson, A. B. Sefkow, D. R. Welch, D. Rose, and C. Olson, Design and characterization of a neutralized-transport experiment for heavy-ion fusion, *Phys. Rev. ST Accel. Beams*, 2004, 7(8): 083501
11. P. K. Roy, S. S. Yu, S. Eylon, E. Henestroza, A. Anders, F. M. Bieniosek, W. G. Greenway, B. G. Logan, W. L. Waldron, D. L. Vanecek, D. R. Welch, D. V. Rose, R. C. Davidson, P. C. Efthimion, E. P. Gilson, A. B. Sefkow, and W. M. Sharp, Results on intense beam focusing and neutralization from the neutralized beam experiment, *Phys. Plasmas*, 2004, 11(5): 2890
12. P. K. Roy, S. S. Yu, S. Eylon, E. Henestroza, A. Anders, E. P. Gilson, F. M. Bieniosek, W. G. Greenway, B. G. Logan, W. L. Waldron, D. B. Shuman, D. L. Vanecek, D. R. Welch, D. V. Rose, R. C. Davidson, P. C. Efthimion, I. D. Kaganovich, A. B. Sefkow, and W. M. Sharp, Drift compression and final focus options for heavy ion fusion, *Nucl. Instrum. Methods Phys. Res. A*, 2005, 544(1–2): 255
13. J. S. T. Ng, P. Chen, H. Baldis, P. Bolton, D. Cline, W. Craddock, C. Crawford, F. J. Decker, C. Field, Y. Fukui, V. Kumar, R. Iverson, F. King, R. E. Kirby, K. Nakajima, R. Noble, A. Ogata, P. Raimondi, D. Walz, and A. W. Weidemann, Observation of plasma focusing of a 28.5 GeV positron beam, *Phys. Rev. Lett.*, 2001, 87(24): 244801
14. H. Qin, R. C. Davidson, J. J. Barnard, and E. P. Lee, Drift compression and final focus options for heavy ion fusion, *Nucl. Instrum. Methods Phys. Res. A*, 2005, 544(1–2): 255
15. R. C. Davidson and H. Qin, Kinetic description of neutralized drift compression and transverse focusing of intense ion charge bunches, *Phys. Rev. ST Accel. Beams*, 2005, 8(6): 064201
16. A. B. Sefkow and R. C. Davidson, Theoretical models for describing longitudinal bunch compression in the neutralized drift compression experiment, *Phys. Rev. ST Accel. Beams*, 2006, 9(9): 090101
17. I. D. Kaganovich, E. A. Startsev, A. B. Sefkow, and R. C. Davidson, Charge and current neutralization of an ion-beam pulse propagating in a background plasma along a Solenoidal magnetic field, *Phys. Rev. Lett.*, 2007, 99(23): 235002
18. M. A. Dorf, I. D. Kaganovich, E. A. Startsev, and R. C. Davidson, Enhanced self-focusing of an ion beam pulse propagating through a background plasma along a Solenoidal magnetic field, *Phys. Rev. Lett.*, 2009, 103(7): 075003
19. T. Namiki, A new FDTD algorithm based on alternating-direction implicit method, *IEEE Trans. Microw. Theory Tech.*, 1999, 47(10): 2003
20. R. W. Hockney and J. W. Eastwood, Computer Simulation Using Particles, New York: McGraw-Hill, 1981
21. J. P. Berenger, A perfectly matched layer for the absorption of electromagnetic waves, *J. Comput. Phys.*, 1994, 114(2): 185
22. J. Villasenor and O. Buneman, Rigorous charge conservation for local electromagnetic field solvers, *Comput. Phys. Commun.*, 1992, 69(2–3): 306
23. M. A. Dorf, I. D. Kaganovich, E. A. Startsev, and R. C. Davidson, Whistler wave excitation and effects of self-focusing on ion beam propagation through a background plasma along a solenoidal magnetic field, *Phys. Plasmas*, 2010, 17(2): 023103